



# Au@Ag@Pt core-shell nanorods regulating Ag release behavior endow titanium antibacterial activity and biocompatibility

Jia-Jun Qiu, Ting-Ting Yang, Yi-Fan Li, Wen-Hao Qian\* , Xuan-Yong Liu\* 

Received: 27 March 2021 / Revised: 19 April 2021 / Accepted: 28 April 2021 / Published online: 19 August 2021  
© Youke Publishing Co., Ltd. 2021

**Abstract** Although titanium and its alloys are extensively used in orthopedics and dentistry fields, implant failures still happen because of implant-associated infections. Herein, Au@Ag@Pt core-shell nanorods with noble metal combination were fabricated and assembled on medical titanium surface and the antibacterial activity and biocompatibility were investigated. The results showed that antibacterial rates of Ti–Au@Ag@Pt against *S. epidermidis* and *P. aeruginosa* were 89.7% and 92.7%, respectively. Besides, Ti–Au@Ag@Pt showed no obvious cell toxicity with MC3T3-E1 cells grew well on the sample surface. It was discovered that the Pt shell layer on Ti–

Au@Ag@Pt slowed down the Ag ion release rate which endowed medical titanium surface with both antibacterial activity and good biocompatibility.

**Keywords** Titanium; Silver; Nanorod; Antibacterial; Biocompatibility

## 1 Introduction

Titanium and its alloys are extensively used in orthopedics and dentistry fields due to their superior physicochemical properties and good biocompatibility [1, 2]. Despite the advantages, implant-associated infection, one of the most severe post-surgery complications, still occurs which will lead to implant failure [3]. To address this problem, it is necessary to endow titanium implants with antibacterial activity. Thus, surface modifications are needed to improve the success rate of titanium implants by introducing antibacterial agents including antibiotics, inorganic, or organic antibacterial coating [4–9].

However, antibiotic resistance has become a public health threat due to the abuse of antibiotics [10]. Compared to antibiotics, silver (Ag) is an inorganic antibacterial agent which has a broad spectrum of antibacterial effect [8]. Owing to their superior inhibitory and biocidal effects, Ag-based antibacterial agents attract wide attention [11–15]. Therefore, Ag-based antibacterial agents, in the form of metallic Ag or Ag ions, have been widely used as bactericides to treat various bacterial infections containing Gram-positive and Gram-negative bacteria. For example, Fan et al. [16] developed an Ag-loaded mesoporous bioactive glass (Ag-MBG) and realized antibacterial effects against *Enterococcus faecalis* in root canal by

---

Jia-Jun Qiu and Ting-Ting Yang have contributed equally to this work.

---

J.-J. Qiu, X.-Y. Liu\*  
School of Chemistry and Materials Science, Hangzhou Institute for Advanced Study, University of Chinese Academy of Sciences, Hangzhou 310024, China  
e-mail: xyliu@mail.sic.ac.cn

J.-J. Qiu, T.-T. Yang, X.-Y. Liu  
State Key Laboratory of High Performance Ceramics and Superfine Microstructure, Shanghai Institute of Ceramics, Chinese Academy of Sciences, Shanghai 200050, China

T.-T. Yang  
School of Materials Science and Engineering, Jiamusi University, Jiamusi 154007, China

Y.-F. Li  
Smart Materials and Surfaces Laboratory, Faculty of Engineering and Environment, Northumbria University, Newcastle upon Tyne NE1 8ST, UK

W.-H. Qian\*  
Shanghai Xuhui District Dental Center, Shanghai 200032, China  
e-mail: pingyanlaoto@163.com



releasing Ag ions from Ag-MBG. Wei et al. [17] prepared TiO<sub>2</sub> nanotubes with long-term antibacterial activity by loading Ag nanoparticles and Ag ions.

Although the antibacterial effects of Ag-based antibacterial agents are proved, challenges remain in their applications in medical implants. It is important to note that the biocompatibility should not be ignored as cytotoxicity was found resulting from Ag nanoparticles or Ag ions [18, 19]. Besides, Ag nanoparticles are easy to aggregate, and they in turn reduces their antibacterial efficiency. To address these issues, in the present work, Au@Ag@Pt core-shell nanorods with the noble metal combination were fabricated on the titanium surface. Au nanorods were acted as the carriers, metallic Ag were uniformly dispersed on the surface of Au nanorods, and Pt shell regulated the release behaviors of Ag ions which endow titanium with both antibacterial activity and good biocompatibility.

## 2 Experimental

### 2.1 Sample preparation

Gold nanorods (GNRs) were fabricated based on a seed-mediated growth method according to our previous work [20]. In brief, seed solutions were obtained after mixing 0.12 ml HAuCl<sub>4</sub> solution (0.02 mol·L<sup>-1</sup>, Aladdin, China), 2.50 ml deionized water and 5.00 ml cetyltrimethylammonium bromide solution (CTAB, 0.10 mol·L<sup>-1</sup>, Aladdin, China), and 0.60 ml NaBH<sub>4</sub> (0.01 mol·L<sup>-1</sup>, Aladdin, China) under magnetic stirring. After vigorous stirring for 2 min, the seed solution was kept at 25–27 °C and aged at least 4 h to allow gas decomposition. Subsequently, 1.50 ml HAuCl<sub>4</sub> solution (0.02 mol·L<sup>-1</sup>), and 0.80 ml silver nitrate solution were introduced into 30 ml CTAB solution (0.10 mol·L<sup>-1</sup>). Then, 0.10 mol·L<sup>-1</sup> ascorbic acid (AA) solution (Aladdin, China) was introduced until the above-mentioned solution turned colorless under magnetic stirring. At last, GNRs were obtained after adding 76 µl as-prepared seed solution and reacted for 12 h.

To prepare Au@Ag core-shell structure nanorods, 55 µl ascorbic acid solution (0.01 mol·L<sup>-1</sup>), 0.20 ml silver nitrate solution (0.01 mol·L<sup>-1</sup>) and 50 µl NaOH (0.10 mol·L<sup>-1</sup>) were introduced to the as-prepared GNRs solution (5.00 ml) with magnetic stirring for 1 h and the corresponding samples were denoted as Au@Ag. Au@Pt core-shell structure nanorods were fabricated by adding 0.90 ml AA solution (0.01 mol·L<sup>-1</sup>) and 20 µl H<sub>2</sub>PtCl<sub>6</sub> solution (18 mmol·L<sup>-1</sup>, Sinopharm Group, China) into 6.00 ml as-prepared GNRs solution and reacting for 1 h under magnetic stirring at 60 °C. The corresponding samples were indicated as Au@Pt. Similarly, to prepare Au@Ag@Pt core-shell structure nanorods, 0.90 ml AA

solution (0.01 mol·L<sup>-1</sup>) and 20 µl H<sub>2</sub>PtCl<sub>6</sub> solution (18 mmol·L<sup>-1</sup>) were added into 6 ml as-prepared Au@Ag solution and reacted for 1 h under magnetic stirring at 60 °C. The corresponding samples were indicated as Au@Ag@Pt.

The self-assembly of GNRs, Au@Ag, Au@Pt, Au@Ag@Pt on medical titanium surfaces is as follows. First, pure titanium plates with the size of 10 mm × 10 mm × 1 mm were cleaned with a mixed acid solution (volume ratio of HF: HNO<sub>3</sub>: H<sub>2</sub>O of 1: 5: 34). To obtain hydroxylated surfaces, these titanium plates were immersed in a piranha solution (volume ratio of H<sub>2</sub>SO<sub>4</sub>: H<sub>2</sub>O<sub>2</sub> of 3: 1) for 3 h. Then, these titanium plates were transferred into 3-aminopropyltrimethoxysilane (APS) solutions (5 vol%, Aladdin, China) and reacted under ultrasonic agitation for 2 h. The APS-treated plates were then transferred into NaCl solution (6 mmol·L<sup>-1</sup>) containing polystyrenesulfonate (PSS, 100 mg·ml<sup>-1</sup>, Aladdin, China) for 24 h with shaking. At last, APS-PSS-treated plates were separately immersed into centrifugal GNRs, Au@Ag, Au@Pt and Au@Ag@Pt solutions and the corresponding samples were labeled as Ti-GNR, Ti-Au@Ag, Ti-Au@Pt and Ti-Au@Ag@Pt, respectively. The titanium plate treated with piranha solution was used as the control group and labeled as Ti.

### 2.2 Surface characterization

Surface morphologies of Au@Ag, Au@Pt and Au@Ag@Pt were observed using transmission electron microscopy (TEM, HRTEM, JSM-6700 F, JEOL, Japan) and the sizes of nanorods were calculated. Scanning electron microscopy (SEM, S-4800, Hitachi, Japan) was utilized to observe the surface topography of Ti, Ti-GNR, Ti-Au@Ag, Ti-Au@Pt and Ti-Au@Ag@Pt. The surface elemental compositions and chemical states of Ti, Ti-GNR, Ti-Au@Ag, Ti-Au@Pt and Ti-Au@Ag@Pt were detected by X-ray photoelectron spectroscopy (XPS, Physical Electronics PHI 5802). The absorption spectra of GNRs, Au@Ag, Au@Pt and Au@Ag@Pt were analyzed using ultraviolet visible near infrared (UV-Vis-NIR) spectrophotometer (Lambda 750, PerkinElmer, USA). The surface contact angles of various samples were measured using a contact angle measurement (SL200B, China). To be specific, 2 µl ultrapure water was dropped on each sample and the photograph was taken with the built-in camera. Water contact angles were obtained after analyzing the photographs.

### 2.3 Ag release assessment

Ti-GNR, Ti-Au@Ag, Ti-Au@Pt and Ti-Au@Ag@Pt were separately immersed into 10 ml ultrapure water at

37 °C for 7 days. The released Ag contents were measured by inductively coupled plasma atomic emission spectroscopy (ICP-AES).

## 2.4 Antibacterial activity analysis

Strains of *Pseudomonas aeruginosa* (*P. aeruginosa*, ATCC 27,853) and *Staphylococcus epidermidis* (*S. epidermidis*, ATCC 12,228) were utilized to assess the antibacterial activities of Ti, Ti-GNR, Ti–Au@Ag, Ti–Au@Pt and Ti–Au@Ag@Pt. *P. aeruginosa* and *S. epidermidis* were cultured with Luria–Bertani broth (LB) and tryptic soy broth (TSB), respectively. Various samples were sterilized under ultraviolet radiation for 12 h. Then, 60 µl bacterial suspensions with a cell density of  $3 \times 10^7$  CFU·ml<sup>-1</sup> were seeded on various samples and cultured for 24 h at 37 °C. For bacteria colony counting, bacteria on the sample surfaces were detached and collected in a 5-ml tube. Then, the detached bacterial suspension was serially diluted tenfold with physiological saline and 100 µl diluted bacterial suspension was transferred to a standard agar culture plate for further cultivation for 24 h. Finally, photographs of agar culture plates were taken and the number of bacteria colonies were counted. The antibacterial rates were calculated according to the following formula:

$$\text{Antibacterial rate} = \frac{N_0 - N_1}{N_0} \times 100\% \quad (1)$$

where  $N_0$  presents the average number of bacteria colonies on the control sample (CFU·ml<sup>-1</sup>) and  $N_1$  indicates the average number of bacteria colonies on the experimental sample.

For SEM bacterial morphology observation, bacteria on the samples were fixed using 2.5% glutaraldehyde and dehydrated with gradient ethanol solutions and hexamethyl disilazane ethanol solution. At last, bacterial morphologies were observed using a scanning electron microscope (SEM, S-3400 N, Hitachi, Japan). To figure out whether Ag ions release led to the antibacterial effect, an agar diffusion assay was carried out. In brief, 100 µl bacterial suspension ( $1 \times 10^8$  CFU·ml<sup>-1</sup>) was introduced to the agar culture plates. Subsequently, Ti, Ti-GNR, Ti–Au@Ag, Ti–Au@Pt and Ti–Au@Ag@Pt were placed on the agar culture plates and cultured at 37 °C for 24 h. At last, photographs of agar culture plates were taken.

## 2.5 Cytocompatibility evaluation

MC3T3-E1 cells (purchased from cells Resource Center, Shanghai Institutes of Biological Science, China) were utilized to investigate the cell viability of various samples. The MC3T3-E1 cells were cultured with Dulbecco's minimum essential medium (DMEM, Gibco, Invitrogen, Inc,

USA) containing 10% fetal bovine serum (FBS, Gibco, Invitrogen, Inc, USA), 1% antimicrobial of penicillin–streptomycin (Antibiotic–Antimycotic, Gibco, Invitrogen, Inc, USA) with 5% CO<sub>2</sub> at 37 °C in a humidified atmosphere. The cell culture medium was refreshed every 3 days. All the samples were sterilized with ultraviolet radiation for 12 h. To evaluate the cell viability of Ti, Ti-GNR, Ti–Au@Ag, Ti–Au@Pt and Ti–Au@Ag@Pt, 1 ml MC3T3-E1 cells ( $4.0 \times 10^4$  cells·ml<sup>-1</sup>) were introduced on various samples and cultured for 1 day. Then, cells on samples were fixed using 2.5% glutaraldehyde and dehydrated with gradient ethanol solutions and hexamethyl disilazane ethanol solution. At last, cell morphologies were observed using SEM (S-3400 N, Hitachi, Japan).

## 2.6 Statistical analysis

All the data were presented as the mean ± standard deviations. Statistical analysis was assessed using GraphPad Prism Software. The statistically significant differences were analyzed using a two-way analysis of variance and Tukey's multiple comparison tests.

# 3 Results and discussion

## 3.1 Surface characterization

TEM and HRTEM images of Au@Ag, Au@Pt and Au@Ag@Pt are shown in Fig. 1. GNR presented a smooth nanorod morphology with the length of  $(49.0 \pm 4.0)$  nm, the width of  $(11.0 \pm 2.0)$  nm, and length/width ( $L/D$ ) ratio of  $\sim 4.3$  [20]. TEM morphology with apparent core–shell nanorod structure can be seen from Au@Ag with the length of  $(55.3 \pm 14.3)$  nm, the width of  $(23.7 \pm 6.3)$  nm, and an  $L/D$  ratio of  $\sim 2.3$ . Components of Au and Ag were detected from Au@Ag by energy-dispersive spectroscopy (EDS) analysis as shown in Table 1. Based on these, it can be concluded that the Ag shell layer has been successfully fabricated on gold nanorod surface. Besides, with the lattice parameters of Au and Ag being similar, there is a smooth and flat interface between the Au core and the Ag shell. Au and Pt were detected from Au@Pt (Table 1), which suggests that Pt can be deposited on gold nanorod surface with chemical reduction method. However, Pt was unevenly distributed on gold nanorod with island structure, as presented in Fig. 1, which is ascribed to the high surface energy and cohesive energy of Pt [21]. Table 1 shows that Au, Ag and Pt were detected from Au@Ag@Pt, which implies that Pt has been successfully deposited on Au@Ag@Pt. Similarly, Pt on Au@Ag@Pt exhibits island structure.

UV–Vis–NIR absorption spectra of GNR, Au@Ag, Au@Pt and Au@Ag@Pt are shown in Fig. 2. Two

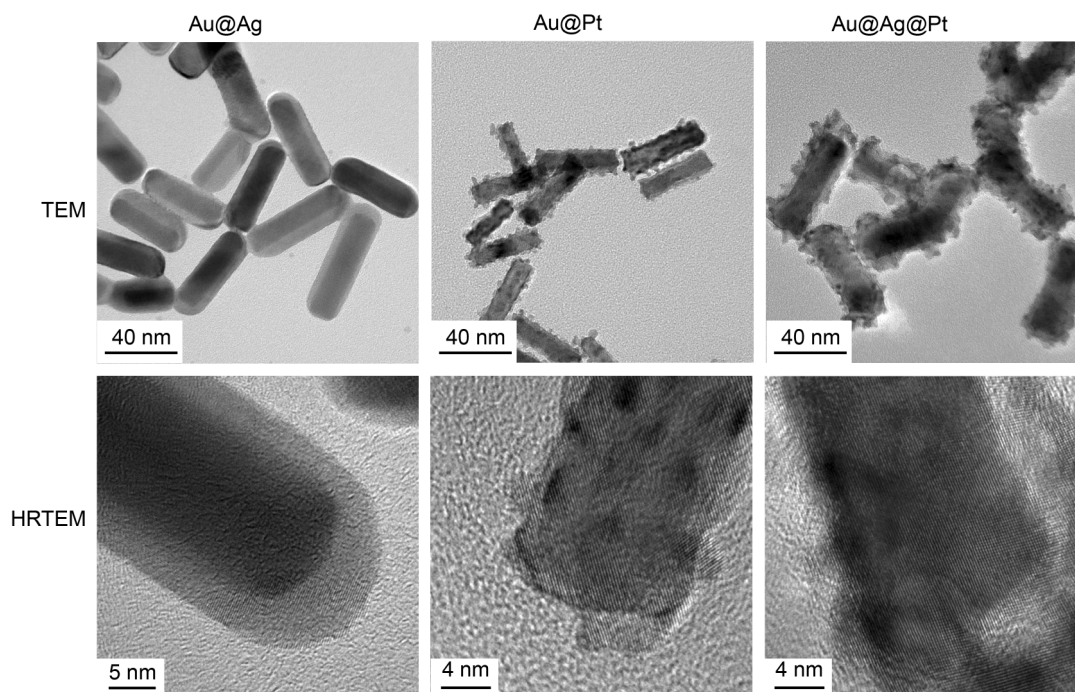


**Fig. 1** TEM and HRTEM images of Au@Ag, Au@Pt and Au@Ag@Pt

**Table 1** EDS component analysis of Ag, Au and Pt from Au@Ag, Au@Pt and Au@Ag@Pt (at%)

Samples	Au	Ag	Pt
Au@Ag	53.52	46.48	–
Au@Pt	75.84	–	24.16
Au@Ag@Pt	48.56	30.13	21.31

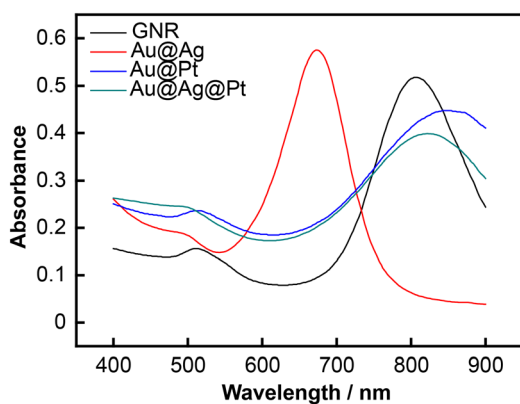


**Fig. 2** UV-Vis-NIR spectra of GNR, Au@Ag, Au@Pt and Au@Ag@Pt

apparent absorption peaks at 520 and 808 nm are observed from GNR corresponding to the transverse plasma resonance absorption peak (TPRAP) and longitudinal plasma

resonance absorption peak (LPRAP), respectively. TPRAP is relatively steady, while LPRAP is susceptible to the changes of physicochemical properties of gold nanorod including surface roughnesses,  $L/D$  ratios, etc. [21]. Compared with GNR, TPRAP of Au@Ag has no significant change while LPRAP shows a blue shift due to the reduction of  $L/D$  ratio. The LPRAP is closely related to  $L/D$  ratio of gold nanorod, and it will show a blue shift with the decrease of  $L/D$  ratio [22]. However, LPRAP of Au@Pt and Au@Ag@Pt exhibits red shift due to the large surface roughness [23].

GNR, Au@Ag, Au@Pt and Au@Ag@Pt were assembled on the titanium surface and corresponding SEM surface morphologies of Ti, Ti-GNR, Ti-Au@Ag, Ti-Au@Pt and Ti-Au@Ag@Pt are presented in Fig. 3. Ti shows a relatively flat surface at low magnification and honeycomb nanostructures can be observed at high magnification due to the etching effect of piranha solution. GNR, Au@Ag, Au@Pt and Au@Ag@Pt are uniformly distributed on the titanium surface where rod-like structures can be seen. XPS full spectra of Ti, Ti-GNR, Ti-Au@Ag, Ti-Au@Pt and Ti-Au@Ag@Pt are shown in Fig. 4a. C is detected from all the samples due to carbon contamination. Ti and O are detected from Ti sample, which may be ascribed to the formation of titanium oxide during the cleaning process using piranha solution. Ag is observed from Ti-Au@Ag and Ti-Au@Ag@Pt, Pt can be seen from Ti-Au@Pt and Ti-Au@Ag@Pt, and Au appears on Ti-GNR, Ti-Au@Ag,

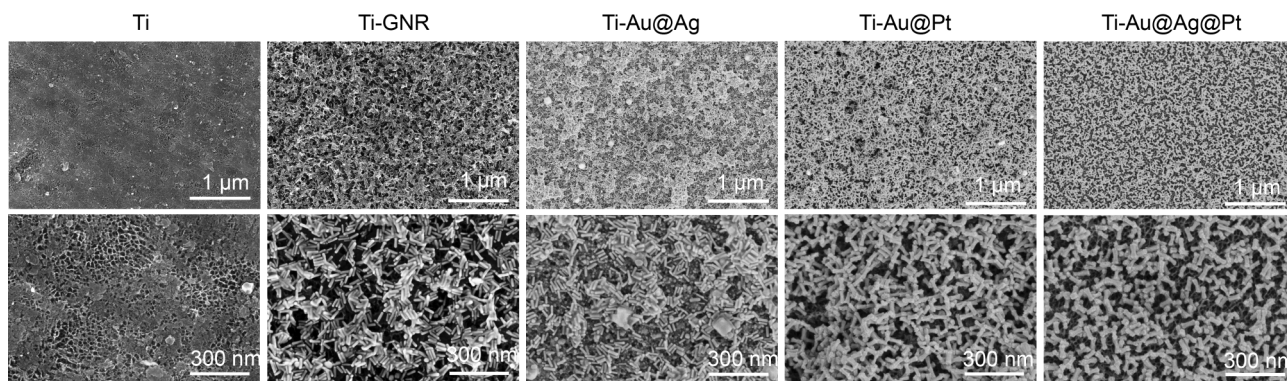


**Fig. 3** SEM images of Ti, Ti-GNR, Ti-Au@Ag, Ti-Au@Pt and Ti-Au@Ag@Pt at low and high magnification

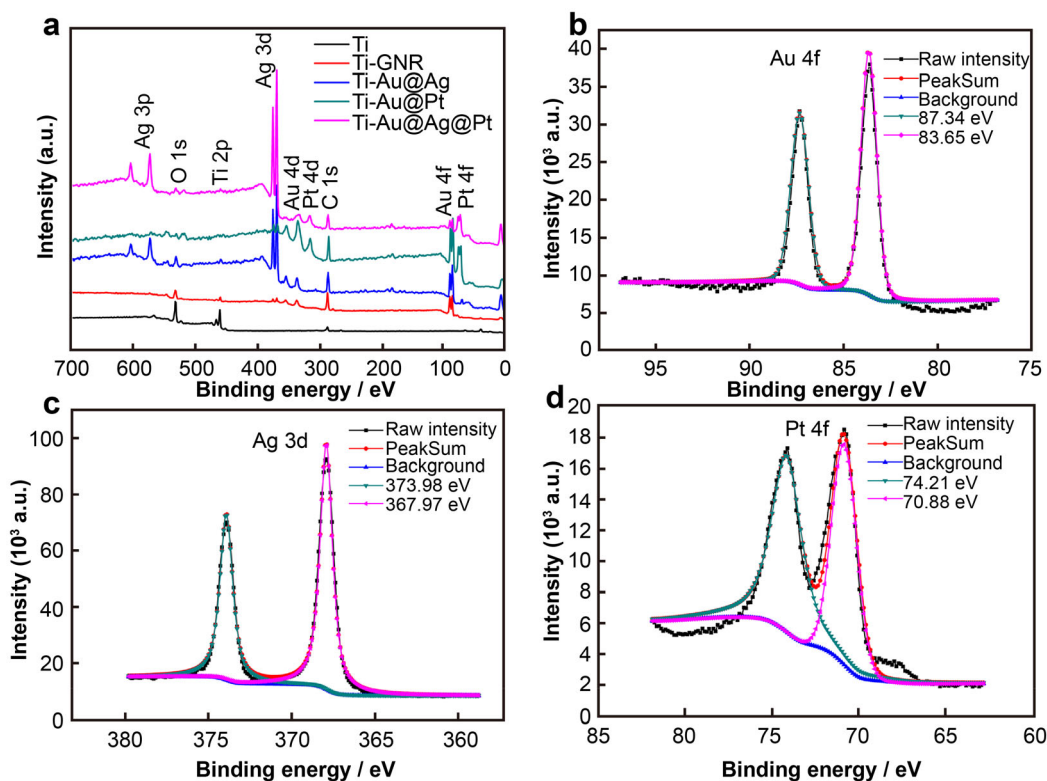


**Fig. 4** a XPS full spectra of Ti, Ti-GNR, Ti-Au@Ag, Ti-Au@Pt and Ti-Au@Ag@Pt; b Au, c Ag and d Pt high-resolution spectra of Ti-Au@Ag@Pt

Ti-Au@Pt and Ti-Au@Ag@Pt. It further confirms that GNR, Au@Ag, Au@Pt and Au@Ag@Pt have been successfully fabricated on the titanium surface. Besides, chemical states of Au, Ag and Pt on Ti-Au@Ag@Pt were investigated and the corresponding results of XPS high-resolution spectra are presented in Fig. 4b–d. Binding energies at 83.6 and 87.3 eV correspond to Au 4f<sub>7/2</sub> and Au 4f<sub>5/2</sub> in metallic gold, respectively [24]. The high-resolution spectra of Ag 3d and Pt 4f also verify the presence of metallic silver and platinum [25, 26].

### 3.2 Surface wettability

Nanorods of GNR, Au@Ag, Au@Pt and Au@Ag@Pt on titanium surface have an effect on the surface wettability, as shown in Fig. 5. Ti exhibits a hydrophilic surface with a contact angle of 4.3° due to the existence of hydroxyl resulting from pickling using piranha solution. Compared with Ti, contact angles of Ti-GNR, Ti-Au@Ag, Ti-Au@Pt and Ti-Au@Ag@Pt increase and there are no significant differences among them.

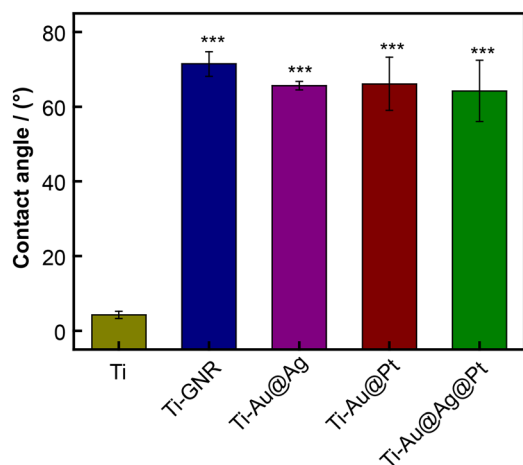


**Fig. 5** Water contact angles of Ti, Ti-GNR, Ti-Au@Ag, Ti-Au@Pt and Ti-Au@Ag@Pt (\*\* $p < 0.001$  vs. Ti)

### 3.3 Ag release analysis

Ag release features from Ti-GNR, Ti-Au@Ag, Ti-Au@Pt and Ti-Au@Ag@Pt within 7 days were investigated. Ag was not detected from Ti-GNR and Ti-Au@Pt. Ag contents released from Ti-Au@Ag and Ti-Au@Ag@Pt with 7 days are  $0.0156$  and  $0.0055 \mu\text{g}\cdot\text{ml}^{-1}$ , respectively. Compared with Ti-Au@Ag, there was less Ag content released from Ti-Au@Ag@Pt. It indicates that the Pt shell layer on Ti-Au@Ag@Pt can regulate Ag ions release in a slow way.

### 3.4 Antibacterial activity assessment

Strains of *S. epidermidis* and *P. aeruginosa* were used to assess the antibacterial activities of Ti, Ti-GNR, Ti-Au@Ag, Ti-Au@Pt and Ti-Au@Ag@Pt and surface morphologies of bacteria cultured on various samples are shown in Fig. 6a. *S. epidermidis* shows a smooth and intact spherical morphology on Ti, which indicates that Ti has no antibacterial activity against *S. epidermidis*. A few *S. epidermidis* with deformed morphology can be observed from Ti-GNR and Ti-Au@Pt, and most *S. epidermidis* grow well on Ti-GNR and Ti-Au@Pt. However, the bacteria numbers of *S. epidermidis* on Ti-Au@Ag and Ti-Au@Ag@Pt were significantly reduced and most *S. epidermidis* were dead with wizened morphology (red arrows), especially for Ti-Au@Ag. It suggests that Ti-Au@Ag and Ti-Au@Ag@Pt have good antibacterial activity against *S. epidermidis*. A similar antibacterial effect can be found on *P. aeruginosa* cultured on Ti, Ti-GNR, Ti-Au@Ag, Ti-Au@Pt and Ti-Au@Ag@Pt for 24 h. *P. aeruginosa* grew well on Ti and a few *P. aeruginosa* with deformed morphology could be found on Ti-GNR and Ti-Au@Pt. However, *P. aeruginosa* on Ti-

Au@Ag and Ti-Au@Ag@Pt were dead with malformed cell morphology, especially for Ti-Au@Ag. To further calculate the antibacterial rates of Ti, Ti-GNR, Ti-Au@Ag, Ti-Au@Pt and Ti-Au@Ag@Pt against *S. epidermidis* and *P. aeruginosa*, plate colony counting was performed and the results are shown in Fig. 6b, c. The antibacterial rates of Ti-GNR, Ti-Au@Ag, Ti-Au@Pt and Ti-Au@Ag@Pt against *S. epidermidis* are 48.0%, 57.0%, 98.0% and 89.7%, respectively. The antibacterial rates of Ti-GNR, Ti-Au@Ag, Ti-Au@Pt and Ti-Au@Ag@Pt against *P. aeruginosa* are 19.3%, 32.9%, 100% and 92.7%, respectively. It indicates that Ti-Au@Ag exhibits the highest antibacterial activity, followed by Ti-Au@Ag@Pt. To further investigate the Ag release antibacterial effect, agar diffusion assay was performed and the results are presented in Fig. 7. Inhibition zones can only be found on Ti-Au@Ag and Ti-Au@Ag@Pt. The inhibition zone diameters of Ti-Au@Ag and Ti-Au@Ag@Pt against *S. epidermidis* were measured at 1.85 and 1.54 cm, respectively, and the inhibition zone diameters of Ti-Au@Ag and Ti-Au@Ag@Pt against *P. aeruginosa* were measured at 3.23 and 2.31 cm, respectively. It implies that Au@Ag and Ti-Au@Ag@Pt can kill bacteria by releasing Ag ions.

Antibacterial mechanisms of Ag-based antibacterial agents have been widely investigated. Cao et al. [25] introduced Ag nanoparticles into titanium substrate using plasma immersion ion implantation technique and demonstrated the controlled antibacterial activity resulting from micro-galvanic effects between Ag nanoparticles and titanium matrix. Nevertheless, many studies reported that released Ag ions from Ag-based antibacterial agents played a vital role in antibacterial activity [27–30]. Ag<sup>0</sup> nanoparticles would not exist long in a realistic environment where H<sup>+</sup> and dissolved O<sub>2</sub> could oxidize Ag<sup>0</sup> nanoparticles to release Ag ions [31]. In this present study, released Ag ions were detected from Ti-Au@Ag and Ti-Au@Ag@Pt, and inhibition zones could also be found around Ti-Au@Ag and Ti-Au@Ag@Pt by agar diffusion assay, confirming the antibacterial mechanism of Ag ions release. Besides, Pt shell layer on Ti-Au@Ag@Pt could regulate Ag ions release in a slow way.

### 3.5 Biocompatibility evaluation

MC3T3-E1 cells were utilized to assess the biocompatibility of Ti, Ti-GNR, Ti-Au@Ag, Ti-Au@Pt and Ti-Au@Ag@Pt and SEM surface morphologies of MC3T3-E1 cells cultured on various samples for 1 day are presented in Fig. 8. A lot of cells adhered on the sample surfaces can be found from Ti, Ti-GNR and Ti-Au@Pt at low magnification, and filopodia and lamellipodia can be seen at high magnification. However, the number of cells

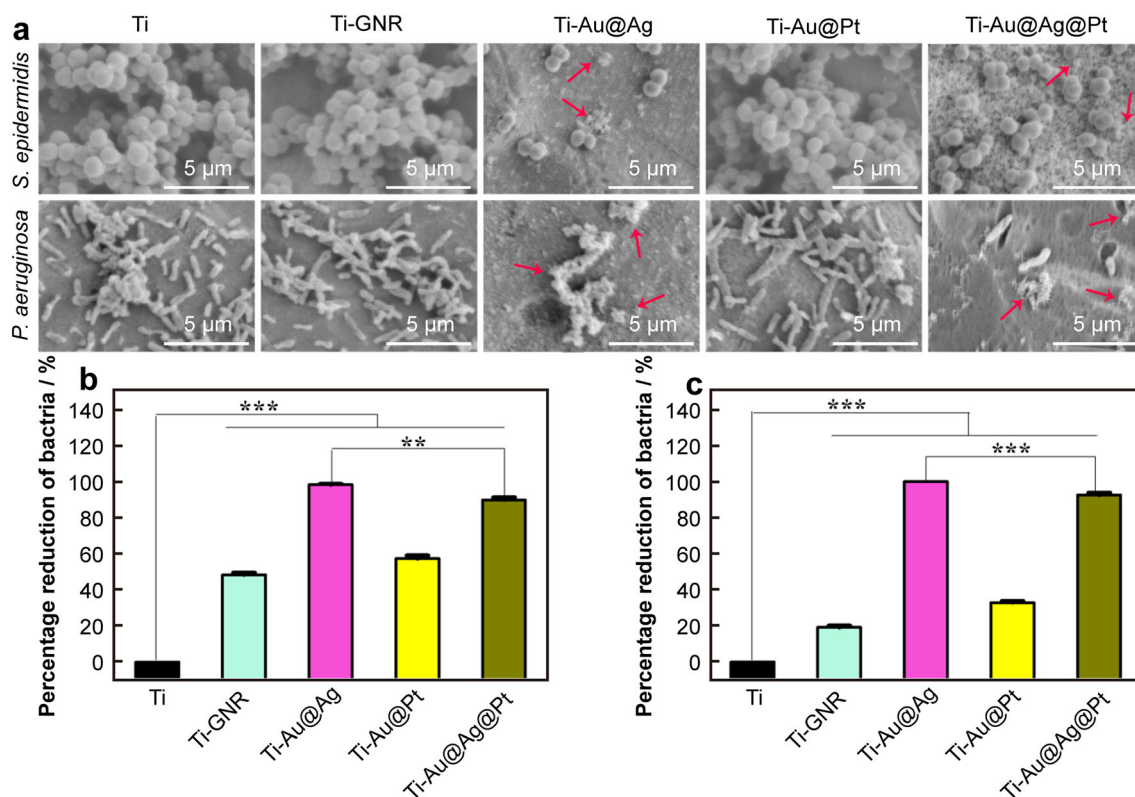


**Fig. 6** a SEM images of *S. epidermidis* and *P. aeruginosa* on Ti, Ti-GNR, Ti-Au@Ag, Ti-Au@Pt and Ti-Au@Ag@Pt, where red arrows indicate damaged bacteria; antibacterial rate of Ti, Ti-GNR, Ti-Au@Ag, Ti-Au@Pt and Ti-Au@Ag@Pt against b *S. epidermidis*, and c *P. aeruginosa* based on the plate colony counting method (\*\* $p < 0.01$ , \*\*\* $p < 0.001$ )

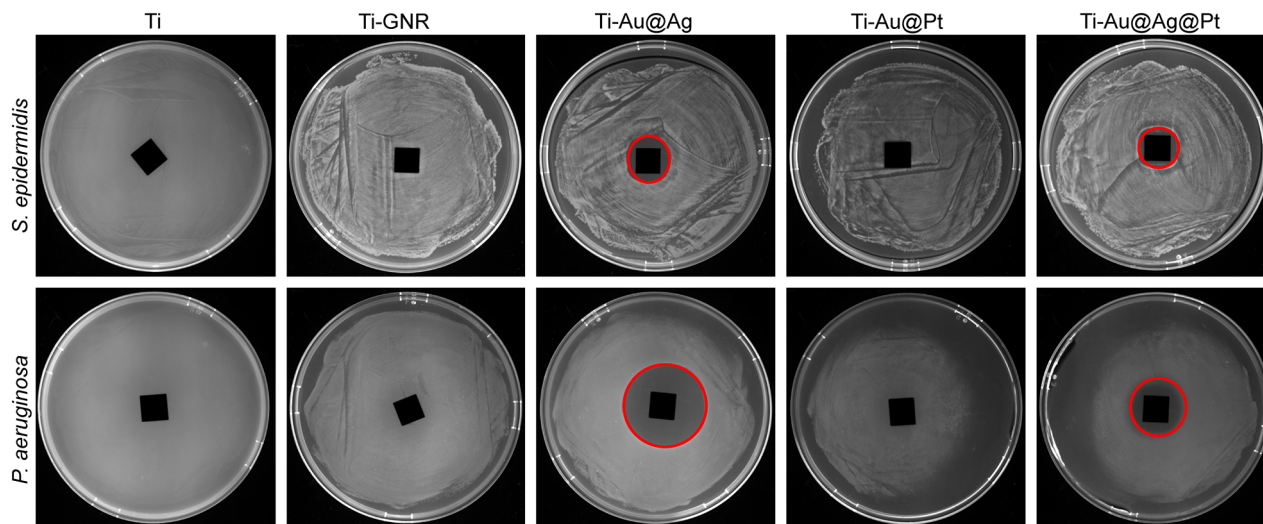


**Fig. 7** Inhibition zones around Ti, Ti-GNR, Ti-Au@Ag, Ti-Au@Pt and Ti-Au@Ag@Pt against *S. epidermidis* and *P. aeruginosa*, where red circle indicates inhibition zone

grown on Ti-Au@Ag was small and cells were almost dead with spherical morphology. Compared with Ti-Au@Ag, the number of cells on Ti-Au@Ag@Pt increased, and filopodia and lamellipodia were observed. Compared

with Ti-Au@Ag, the Pt shell layer on Ti-Au@Ag@Pt slows down the Ag ions release rate. Therefore, Ti-Au@Ag@Pt shows no obvious cell toxicity where MC3T3-E1 cells grow well on sample surface.

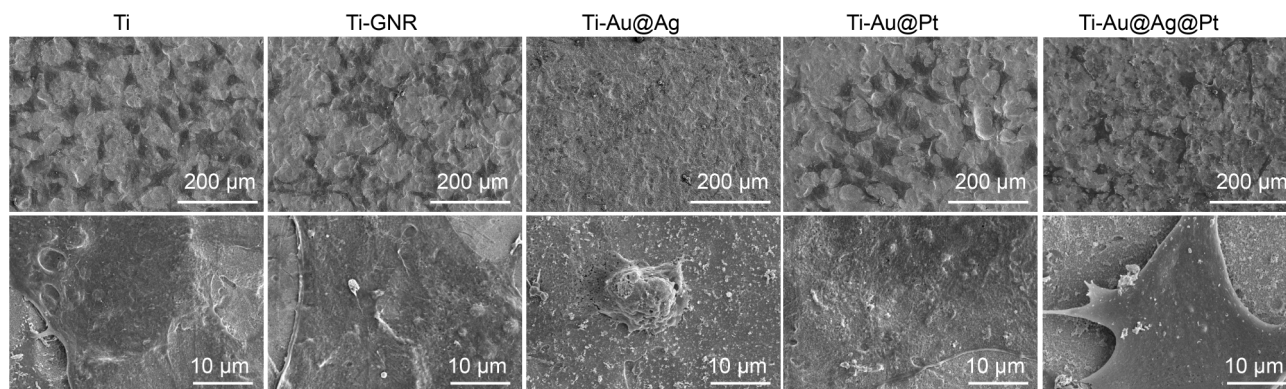


Fig. 8 SEM images of MC3T3-E1 cells cultured on Ti, Ti-GNR, Ti-Au@Ag, Ti-Au@Pt and Ti-Au@Ag@Pt for 1 day

#### 4 Conclusion

In summary, Au@Ag@Pt core-shell nanorods were fabricated on the titanium surface. Compared with Ti-Au@Ag, Ti-Au@Ag@Pt remained the antibacterial activities against *S. epidermidis* and *P. aeruginosa*. Moreover, Ti-Au@Ag@Pt shows no obvious cell toxicity where MC3T3-E1 cells grow well on the sample surface. Pt shell layer on Ti-Au@Ag@Pt slows down the Ag ion release rate which endows medical titanium surface both antibacterial activity and good biocompatibility.

**Acknowledgements** This study was financially supported by the National Natural Science Foundation of China (No. 51831011), Shanghai Scientific and Technological Innovation Project (No. 20ZR1452200), the Program for Outstanding Medical Academic Leader (No. 2019LJ27), the PhD Research Startup Foundation of Jiamusi University (No. JMSUBZ2019-09), Shanghai Medical Key Specialty (No. ZK2019B12) and China Postdoctoral Science Foundation (No. 2019M661642).

#### Declarations

**Conflicts of interests** The authors declare that they have no conflict of interests.

#### References

- [1] Liu XY, Chu PK, Ding CX. Surface modification of titanium, titanium alloys, and related materials for biomedical applications. *Mater Sci Eng R*. 2004;47(3–4):49.
- [2] Zhang JM, Sun YH, Zhao Y, Liu YL, Yao XH, Tang B, Hang RQ. Antibacterial ability and cytocompatibility of Cu-incorporated Ni-Ti-O nanopores on NiTi alloy. *Rare Met*. 2019;38(6):552.
- [3] Liu JQ, Liu J, Attarilar S, Wang C, Tamaddon M, Yang CL, Xie KG, Yao JG, Wang LQ, Liu CZ, Tang YJ. Nano-modified titanium implant materials: a way toward improved antibacterial properties. *Front Bioeng Biotech*. 2020;8:576969.
- [4] Ständert V, Borchering K, Bormann N, Schmidmaier G, Grunwald I, Wildemann B. Antibiotic-loaded amphora-shaped pores on a titanium implant surface enhance osteointegration and prevent infections. *Bioact Mater*. 2021;6(8):2331.
- [5] Qian WH, Qiu JJ, Su JS, Liu XY. Minocycline hydrochloride loaded on titanium by graphene oxide: an excellent antibacterial platform with the synergistic effect of contact-killing and release-killing. *Biomater Sci*. 2018;6(2):304.
- [6] Qiu JJ, Liu L, Zhu HQ, Liu XY. Combination types between graphene oxide and substrate affect the antibacterial activity. *Bioact Mater*. 2018;3(3):341.
- [7] Yan X, Li S, Bao J, Zhang N, Fan B, Li R, Liu X, Pan YX. Immobilization of highly dispersed Ag nanoparticles on carbon nanotubes using electron-assisted reduction for antibacterial performance. *ACS Appl Mater Interfaces*. 2016;8(27):17060.
- [8] Xu Z, Li M, Li X, Liu X, Ma F, Wu S, Yeung KWK, Han Y, Chu PK. Antibacterial activity of silver doped titanate nanowires on Ti implants. *ACS Appl Mater Interfaces*. 2016;8(26):16584.
- [9] Qiu JJ, Wang DH, Geng H, Guo JS, Qian S, Liu XY. How oxygen-containing groups on graphene influence the antibacterial behaviors. *Adv Mater Interfaces*. 2017;4(15):1700228.
- [10] Frieri M, Kumar K, Boutin A. Antibiotic resistance. *J Infect Public Health*. 2017;10(4):369.
- [11] Shang J, Sun Y, Zhang T, Liu Z, Zhang H. Enhanced antibacterial activity of Ag nanoparticle-decorated ZnO nanorod arrays. *J Nanomater*. 2019;2019:3281802.
- [12] Liu Q, Li J, Zhong X, Dai Z, Lu Z, Yang H, Chen R. Enhanced antibacterial activity and mechanism studies of Ag/Bi<sub>2</sub>O<sub>3</sub> nanocomposites. *Adv Powder Technol*. 2018;29(9):2082.
- [13] Chen CC, Wu HH, Huang HY, Liu CW, Chen YN. Synthesis of high valence silver-loaded mesoporous silica with strong antibacterial properties. *Int J Environ Res Public Health*. 2016;13(1):99.
- [14] Chen B, Jiang Y, Zhao M, Wang W, Chu Z, Huo R, Hu F, Zhou W, He T, Qian H. Ag nanoparticles decorated hybrid microspheres for superior antibacterial properties. *Mater Lett*. 2020;262:127057.
- [15] Zhang M, Qiu JJ, Yin T, Tan CL. Research progress and application prospect of silver nanoparticles and nanoporous silver materials. *Chin J Rare Metals*. 2020;44(1):79.
- [16] Fan W, Wu D, Ma T, Fan B. Ag-loaded mesoporous bioactive glasses against *Enterococcus faecalis* biofilm in root canal of human teeth. *Dent Mater J*. 2015;34(1):54.
- [17] Wei L, Wang H, Wang Z, Yu M, Chen S. Preparation and long-term antibacterial activity of TiO<sub>2</sub> nanotubes loaded with Ag nanoparticles and Ag ions. *RSC Adv*. 2015;5(91):74347.
- [18] Yang XY, Gondikas AP, Marinakos SM, Auffan M, Liu J, Hsu-Kim H, Meyer JN. Mechanism of silver nanoparticle toxicity is dependent on dissolved silver and surface coating in *Caenorhabditis elegans*. *Environ Sci Technol*. 2012;46(2):1119.
- [19] Xiu ZM, Zhang QB, Puppala HL, Colvin VL, Alvarez PJJ. Negligible particle-specific antibacterial activity of silver nanoparticles. *Nano Lett*. 2012;12(8):4271.

- [20] Yang T, Wang D, Liu X. Assembled gold nanorods for the photothermal killing of bacteria. *Colloids Surf B*. 2019;173:833.
- [21] Bus E, van Bokhoven JA. Electronic and geometric structures of supported platinum, gold, and platinum—gold catalysts. *J Phys Chem C*. 2007;111(27):9761.
- [22] Chen HJ, Shao L, Li Q, Wang JF. Gold nanorods and their plasmonic properties. *Chem Soc Rev*. 2013;42(7):2679.
- [23] Hu XN, Zhao YY, Hu ZJ, Saran A, Hou S, Wen T, Liu WQ, Ji YL, Jiang XY, Wu XC. Gold nanorods core/AgPt alloy nanodots shell: a novel potent antibacterial nanostructure. *Nano Res*. 2013;6(11):822.
- [24] Yu JG, Yue L, Liu SW, Huang BB, Zhang XY. Hydrothermal preparation and photocatalytic activity of mesoporous Au–TiO<sub>2</sub> nanocomposite microspheres. *J Colloid Interface Sci*. 2009;334(1):58.
- [25] Cao HL, Liu XY, Meng FH, Chu PK. Biological actions of silver nanoparticles embedded in titanium controlled by micro-galvanic effects. *Biomaterials*. 2011;32(3):693.
- [26] Kerrec O, Devilliers D, Groult H, Marcus P. Study of dry and electrogenerated Ta<sub>2</sub>O<sub>5</sub> and Ta/Ta<sub>2</sub>O<sub>5</sub>/Pt structures by XPS. *Mater Sci Eng B*. 1998;55(1–2):134.
- [27] Saint-Cricq P, Wang JZ, Sugawara-Narutaki A, Shimojima A, Okubo T. A new synthesis of well-dispersed, core-shell Ag@SiO<sub>2</sub> mesoporous nanoparticles using amino acids and sugars. *J Mater Chem B*. 2013;1(19):2451.
- [28] Li C, Wang XS, Chen F, Zhang CL, Zhi X, Wang K, Cui DX. The antifungal activity of graphene oxide-silver nanocomposites. *Biomaterials*. 2013;34(15):3882.
- [29] Gao N, Chen YJ, Jiang J. Ag@Fe<sub>2</sub>O<sub>3</sub>-GO nanocomposites prepared by a phase transfer method with long-term antibacterial property. *ACS Appl Mater Interfaces*. 2013;5(21):11307.
- [30] Yan X, Li S, Pan Y, Xing B, Li R, Jang BWL, Liu X. Tunable Ag<sup>+</sup> ion release from Ag@C for antibacterial and antifouling performances. *RSC Adv*. 2015;5(49):39384.
- [31] Liu JY, Hurt RH. Ion release kinetics and particle persistence in aqueous nano-silver colloids. *Environ Sci Technol*. 2010;44(6):2169.